Analysis of the wave propagation properties of a periodic array of rigid cylinders perpendicular to a finite impedance surface

2011 EPL 96 44003

(http://iopscience.iop.org/0295-5075/96/4/44003)

A Letters Journal Exploring the Frontiers of Physics

November 2011

EPL, **96** (2011) 44003
doi: 10.1209/0295-5075/96/44003

www.epljournal.org

Analysis of the wave propagation properties of a periodic array of rigid cylinders perpendicular to a finite impedance surface

V. Romero-García[1], J. V. Sánchez-Pérez[2(a)] and L. M. Garcia-Raffi[3]

[1] *Instituto de Investigación para la Gestión Integrada de zonas Costeras, Universidad Politécnica de Valencia Paraninf 1, 46730 Gandia, Spain, EU*
[2] *Centro de Tecnologías Físicas: Acústica, Materiales y Astrofísica, Universidad Politécnica de Valencia Camino de Vera s/n, 46022 Valencia, Spain, EU*
[3] *Instituto Universitario de Matemática Pura y Aplicada, Universidad Politécnica de Valencia Camino de Vera s/n, 46022 Valencia, Spain, EU*

received 8 August 2011; accepted in final form 3 October 2011
published online 9 November 2011

PACS 43.20.+g – General linear acoustics
PACS 43.35.+d – Ultrasonics, quantum acoustics, and physical effects of sound

Abstract – The effect of the presence of a finite impedance surface on the wave propagation properties of a two-dimensional periodic array of rigid cylinders with their axes perpendicular to the surface is both numerically and experimentally analyzed in this work. In this realistic situation the incident wave interacts with two elements: the surface and the array of scatterers. The excess attenuation and the bandgap effects, due to the existence of the surface and the periodicity of the array, respectively, are fundamental to control both the transmission and attenuation of waves on devices based on periodicity.

Introduction. – Research on the transmission properties of Phononic Crystals (PC) [1,2], defined as periodic lattices of elastic scatterers embedded in an elastic medium with different physical properties, has attracted increasing interest in the last decade. Exhaustive studies have been performed in order to know the underlying physics in their main properties of sonic and elastic waves. Refraction [3–5], invisibility [6], bandgaps [7,8], or recently, self-collimation of acoustic beams [9] or control of phase properties [10], are some topics related to the exploitation of the wave propagation properties of PC. In these years, several theoretical methods have been developed to analyze the physical properties of these systems. The Plane Wave Expansion method (PWE) [11] makes use of the periodicity to calculate the band structures of the PC transforming the wave equation into an eigenvalue problem that can be solved for each Bloch vector $\vec{k}$, in the irreducible first Brillouin zone. The Extended Plane Wave Expansion (EPWE) [12,13] is a general method for analyzing the complex dispersion relation of PC solving for the inverse problem, $k(\omega)$. On the other hand, a generalization of the Rayleigh method [14] based on a multipole scattering approach has been developed by Poulton *et al.* [15] to analyze the elastic wave propagation through a two-dimensional array of circular voids. This algorithm has been generalized to the oblique incidence using a canonical representation for the eigenfields associated with the spectral problem [16–18]. The transmission problem in finite structures can be solved using the Multiple Scattering Theory (MST) [19–23], which is a self-consistent method to estimate the acoustic pressure in a point taking into account the incident pressure on the finite PC and the scattering due to all the scatterers. Finally, numerical methods as Finite Difference Time Domain (FDTD) [24] or the Finite Elements Method (FEM) [25] in the frequency domain, can be used to characterize periodic media with either complex geometries of the scatterers or with several coupled effects in addition to scattering.

In a real situation, scatterers should be held on a finite impedance surface and the reflections of both, the incident and the scattered waves on this surface have to be taken into account when the transmission properties of PC are analyzed. However, this effect has not been considered in the previous models. As a first approximation to this problem, recent works [26,27] present both semi-analytical and numerical models to analyze the influence of a finite impedance surface on the transmission

(a) E-mail: jusanc@fis.upv.es

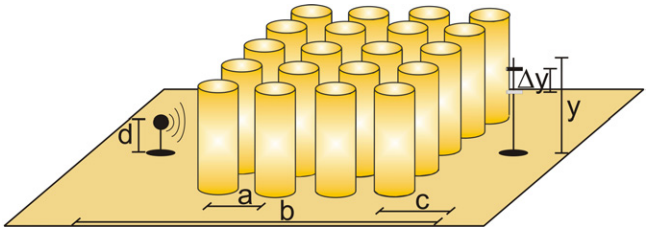

Fig. 1: (Color online) Experimental setup used.

properties of arrays of rigid cylindrical scatterers embedded in air, usually called Sonic Crystals (SC), with their axes parallel to the surface (horizontal scatterers). This situation has the most tractable geometry to develop a semi-analytic model. However, as we have mentioned, the real case involves arrays of cylinders with their axes perpendicular to the surface which means a three-dimensional (3D) geometry problem. This case implies to assume the complete geometry of the composite resulting in complex analytical developments. On the other hand, numerical simulations of these 3D geometries would imply a long computational time.

The goal of this work is to present numerical predictions and experimental results to show the variation of the transmission properties of SC devices when the cylinders are perpendicular to the finite impedance surface. To do this we develop a simplified 3D numerical model based on FEM and we check the results with accurate experimental results obtained in controlled conditions. The interaction between the excess attenuation effect, due to the interference produced by the superposition of the incident wave and the wave reflected by the surface, and the bandgap, due to the periodicity of the array, has been found of fundamental interest for the design of devices based on periodic arrays devoted to control the transmission of waves. The study is focused on the airborne transmission case. The results obtained here allow to enhance the knowledge about the acoustical properties of these systems in a more realistic way.

The work is organized as follows: The experimental setup and the numerical model are presented in the first part of the work, showing the main definitions used through the analysis. Then a discussion about the numerical predictions and the comparison with the experimental results is shown. Finally, we present the concluding remarks of the work.

Experimental setup and numerical analysis. –

Experimental setup. The experimental results have been obtained under controlled conditions in an echo-free chamber sized $8 \times 6 \times 3\,\mathrm{m}^3$. In fig. 1 one can observe the experimental setup used. We have constructed a SC made of 20 (5×4) acoustically rigid cylinders with radius $r = 0.09\,\mathrm{m}$ and 1.20 m length, arranged in a square array with lattice constant $a = 0.22\,\mathrm{m}$. With this geometry the dimensions of the sample are $1.28 \times 1.06 \times 1.20$ and they perfectly fit in the echo-free chamber. The first pseudogap at ΓX direction (0° of incidence) appears between 500 and 980 Hz, as we will explain later.

Two types of surfaces have been considered. The first one is a 0.03 m thick wooden board, theoretically considered as an acoustic rigid surface. The second one is a 0.1 m foam sheet, considered as a porous material with finite impedance characterized with a flow resistivity $\sigma_e = 250\,\mathrm{kPa\,s/m}^2$ and a porosity at the surface $\alpha_e = 1\,\mathrm{m}^{-1}$. To experimentally study the interaction between the SC and the surface, we have taken measurements on a vertical line of points with length $y = 1\,\mathrm{m}$ (starting at 0.05 m from the surface) behind to the SC, as one can see in fig. 1. We have measured this line in steps of $\Delta y = 0.02\,\mathrm{m}$ in order to analyze in depth the interaction between the surfaces and the bandgaps of SC by varying the height of the microphone. The distance between the vertical line of measurements and the center of the nearest row of cylinders is $c = 0.5\,\mathrm{m}$, and the horizontal distance between the sound source and the measurement line is $b = 2.51\,\mathrm{m}$. A source emitting continuous white noise is placed at $d = 0.3\,\mathrm{m}$ distance from the ground.

In our experimental setup, the temporal signal is acquired by a prepolarized free-field microphone $1/2''$ Type 4189 B&K. The microphone position is varied by using a Cartesian robot which controls the movement along the three axes (OX, OY and OZ), installed in the ceiling of the echo-free chamber. The robot is called by us 3DReAMS (3D Robotized e-Acoustic Measurement System), and it has been designed to sweep the microphone through a 3D grid of measuring points located at any trajectory inside the chamber. When the robotized system is turned off, the microphone acquires the temporal signal. This signal is saved on the computer and then, using the Fast Fourier Transform (FFT), one can obtain the frequency response of the measured sample. National Instruments cards PCI-4474 and PCI-7334 have been used together with the Sound and Vibration Toolkit and the Order Analysis Toolkit for LabVIEW for both the data acquisition and the motion of the robot.

Numerical analysis: finite element method. To numerically solve the problem we consider the geometry shown in fig. 2(a). A line source is located at point $\vec{r}_0 = (x, y)$. The emitted acoustic field by this source at point $\vec{r}$ is $p_0 = H_0(k|\vec{r} - \vec{r_0}|)$, where $H_0(x)$ is the Hankel function of the first kind and zeroth order. The numerical domain where the solution is obtained, is formed by a row of 4 scatterers separated by the lattice constant of the array, a, and enclosed between two completely reflecting walls which are parallel to the axis of the scatterers. These walls are also separated by a lattice constant, a. It is worth noting that the incident wave is not reflected by these walls; however, the scattered waves from the cylinders are reflected by the walls reproducing the effect of a semi-infinite periodic slab of 4 rows of scatterers. Then a reduced volume is used here to reproduce the effect of a semi-infinite structure. This

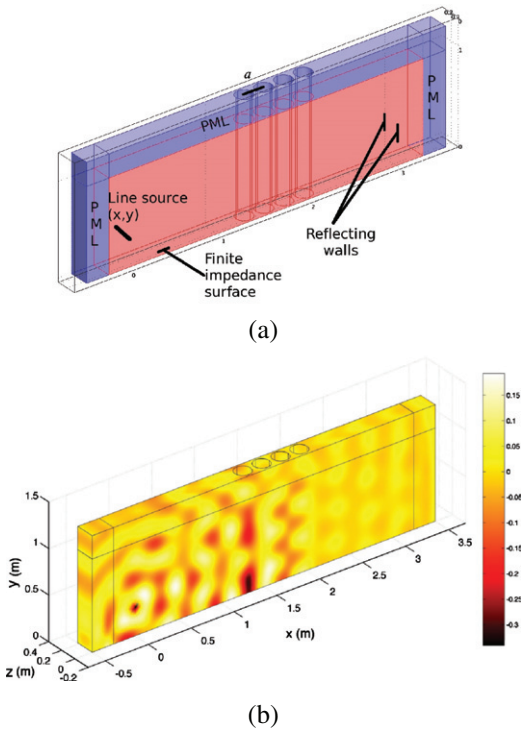

Fig. 2: (Color online) (a) Numerical solution domain. (b) Numerical simulation for the scattering problem with completely rigid ground at 1000 Hz. The real value of the total pressure is plotted, $Re(P)$.

procedure is only valid for plane waves and line sources emitting cylindrical waves.

The numerical domain is surrounded by Perfectly Matched Layers (PML) [28] which are an efficient alternative for emulating the Sommerfeld radiation condition in the numerical solution of the scattering problems. The scatterers are considered acoustically rigid and as a consequence the Neumann boundary conditions (zero sound velocity) are applied in their surfaces. Finally, the finite impedance surface where the cylinders are held is modeled using the impedance boundary condition introducing the expression of the acoustic impedance of the ground. In this work we have characterized the surfaces using a two-parameter impedance model [29] with flow resistivity σ_e and porosity at the surface α_e, being the impedance of the ground

$$Z_{ground} = \rho c_0 \left(0.434\sqrt{\frac{\sigma_e}{\nu}}(1+\imath) + 9.75\imath\frac{\alpha_e}{\nu}\right), \quad (1)$$

where ρ and c_0 are the density and the sound velocity of air, respectively.

We solve the problem for the scattered waves p_s because the incident wave p_0 is itself solution of the wave equation. Thus, the total acoustic field is obtained adding the incident wave to the scattered one. As a consequence of the procedure, the PML only acts on the scattered wave. The commercial software COMSOL 3.5.a is used in this work to obtain the numerical predictions. The solved problem has 10^5 degrees of freedom and $83.7 \cdot 10^4$ elements have been used to solve it. An example of the numerical solution at 1000 Hz is shown in fig. 2(b).

The situation without the SC is very well known: the total field can be characterized by both the incident and the reflected waves on the finite impedance surface (ground). This last one can be obtained using the reflection coefficient of the surface and the image method. Then, without the SC, the total acoustic field is (see ref. [26] for details)

$$p_{tot} = p_0 + p_s, \quad (2)$$

where p_0 is the incident wave and $p_s = R(\vec{r}_0, \vec{r}; \nu)H_0(k|\vec{r'} - \vec{r'}_0|)$ represents the reflected one being $R(\vec{r}_0, \vec{r}; \nu)$ the reflection coefficient of the finite impedance surface. All the vectors measured from the image source are characterized by a prime ($'$). Using these definitions, the excess attenuation (EA) spectrum in the receiver site is characterized using the following expression:

$$EA = \frac{20\log(|p_{tot}|)}{20\log(|p_0|)} = \frac{PL}{PL_0}. \quad (3)$$

The EA spectrum can be obtained analysing the ratio of the total sound level at the receiver (PL) to the direct sound that would be present in the absence of the ground surface (PL_0). Thus, the destructive interference effect between the incident wave and the reflected one on the surface produces minima of PL and, as a consequence, dips in the EA spectrum. These dips depend on both the relative distance between the source and the receiver and on the properties of the surface.

On the other hand, considering now the presence of the SC, the parameter used in this work to characterize the attenuation properties of the complete system (SC and finite impedance surface) is the Insertion Loss (IL), defined here as the difference between the sound level recorded with and without the SC, considering always the presence of the finite impedance surface. Then,

$$IL = 20\log\left(\frac{|p_{tot}|}{|P|}\right), \quad (4)$$

where P is the total acoustic field with both the surface and the SC. We would like to remark that we have taken as reference for the IL the situation where the surface is present.

Sometimes the dispersion relation of the periodic system is useful to compare the effect of the finite size on the scattering problems. Thus, the band structures of the designed SC have been also calculated using the PWE. 961 plane waves have been used in the calculation as this number produced a good convergence of the method for the case analyzed here. We fix our attention in the range of frequencies included in the first pseudogap at ΓX direction due to the fact that, for the lattice constant we are dealing with, these frequencies have important relevance in the field of the acoustic barriers which is perhaps the most exploited application of SC for audible noise.

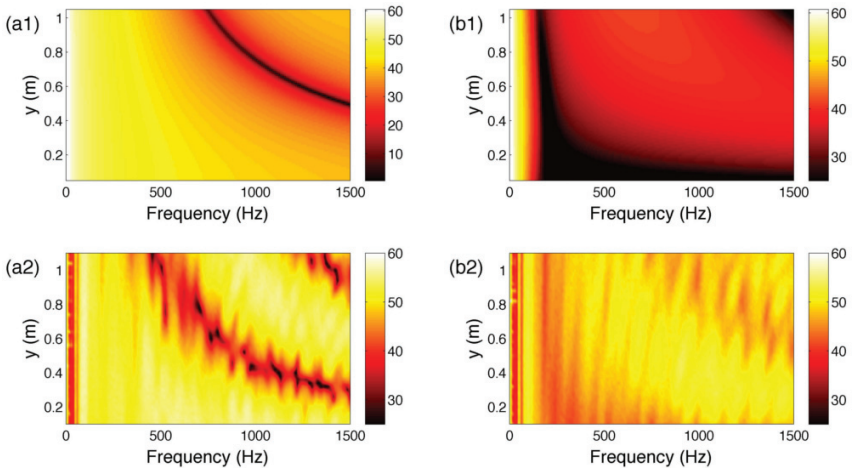

Fig. 3: (Color online) PL, Theoretical analysis in free-field conditions for a rigid surface (a1) and finite impedance surface (b1). PL Experimental measurements performed with 3DReAMS for the two previous cases: rigid surface (a2) and finite impedance surface (b2). The geometrical conditions of both the theoretical and the experimental results have been defined in the second section.

Results and discussion. – First of all we analyze the case of the finite impedance surface without the SC. Figure 3 shows both numerical predictions (1) and experimental results (2) of the PL without the SC, showing the dips of the EA spectrum. One observes the dependence of the dips of the EA spectrum on the height of the measurement point and on the frequency for the rigid a) and absorbent b) surfaces.

On the other hand, in fig. 3 one can check the fairly good agreement between the numerical and the experimental results, as a proof of the accurate precision of our experimental setup. The existing differences in the maps for the case of the rigid surface can results because of the assumption of an acoustically rigid surface for the numerical predictions. In the experimental setup the material used is wood and it does not behave as a completely rigid material. In the case of the finite impedance material, the existing differences between numerical predictions and experimental results can result from the limitations of the impedance model considered here. Note that in this last case, the dips of the EA appear at lower values of both frequencies and heights than in the case of rigid ground.

Once the EA of the surface is characterized we analyze the interaction between SC and both the rigid and the absorbent surfaces. Figures 4(a1) and (a2) show the numerical predictions and the experimental results, respectively, for the case of the acoustically rigid surface. In these figures one can see that the maximum values of the IL appear inside the range of frequencies corresponding to the first band gap at ΓX direction, represented in the figures with the vertical dashed lines as a prolongation of the edges of the bandgap shown in the band structures calculated using PWE method. For this case the interaction produces a positive effect on the EA spectrum of the surface, that means, an increasing of the attenuation properties of the surface. On the other hand, there are some regions on the map where the IL is negative for both several heights and frequencies, which mean a reinforcement of the pressure level compared to

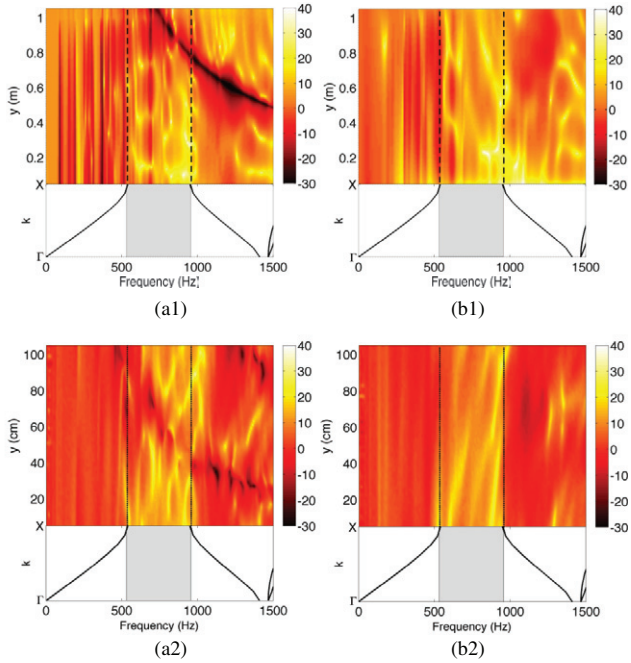

Fig. 4: (Color online) IL theoretical analysis of the SC-rigid surface interaction (a1) and SC-finite impedance surface interaction (b1). Experimental results obtained with 3DReAMS for the two previous cases: SC-rigid surface (a2) and SC-finite impedance surface (b2). The band structures have been calculated using the PWE method, with the following parameters: $\rho_{cylinders} = 2700\,\mathrm{kg/m^3}$, $\rho_{air} = 1.3\,\mathrm{kg/m^3}$; $c_{cylinders} = 6400\,\mathrm{m/s}$ and $c_{air} = 340\,\mathrm{m/s}$, and with 961 plane waves. We have focused our attention on the properties of the first band gap at ΓX, between 500 and 980 Hz.

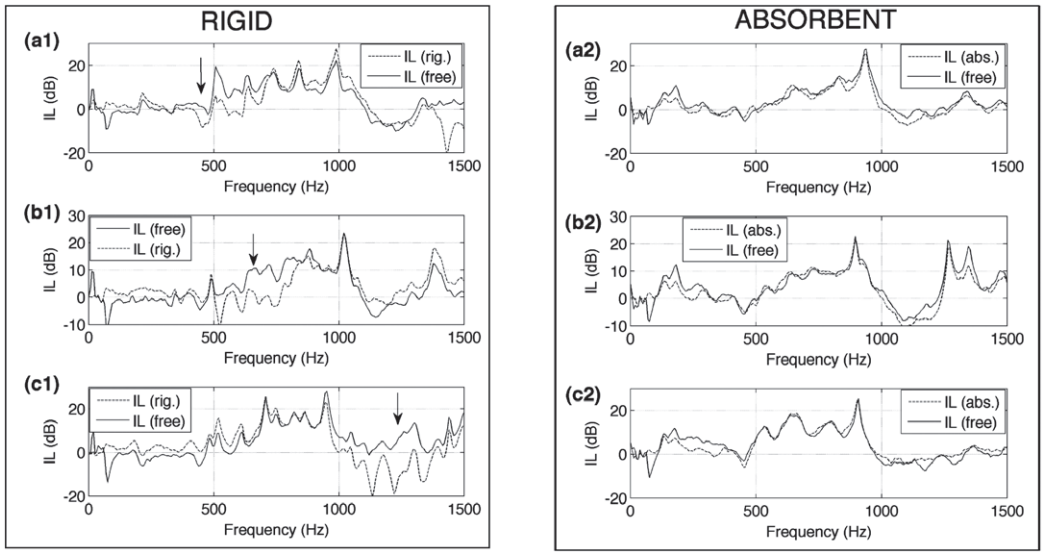

Fig. 5: Experimental IL spectra for three heights of the microphone ($y = 91$ cm (a); $y = 65$ cm (b) and $y = 31$ cm (c)). Continuous and dashed lines represent the IL of SC without ground and with ground, respectively. Figure marked with 1 (2) represents the measurements for rigid (absorbent) ground. One can see, in the case of the rigid surface, its effect on the attenuation properties of SC (marked with arrows). In the case of a finite impedance surface, the existence of the surface does not affect the SC attenuation properties.

the case of rigid surface alone which is considered as the reference. Note that this reinforcement is produced by the combined effect of the SC and the surface, and it means that the attenuation level is lower than in the case of the rigid surface alone, although some attenuation still exists compared with the free-field conditions.

Similar effects can be seen in figs. 4(b1) and (b2) for the case of finite impedance surface. The range of frequencies where the IL is higher is included in the limits of the band gap at ΓX direction, marked with vertical dashed lines. Moreover, some regions in the map show a reinforcement of the acoustical level, although here the size of these areas is lower than in the rigid surface case. All these results are in good agreement with the theoretical predictions shown in [26,27] for the SC-surfaces interaction in the two-dimensional case (horizontal cylinders). The discrepancies observed between the experimental results and the numerical predictions in fig. 4 can result from the size of the sample in the numerical simulation. For this case the sample is semi-infinite while in the experimental results the sample is finite (5×4 scatterers). Even though the presence of the dips in the EA spectrum and the bandgap can be compared.

Up to now, we have compared the dependence of the EA on the different types of surfaces when a SC is introduced. In fig. 5 we show the opposite analysis that explains the influence of the impedance of the surfaces on the attenuation properties of SC. In this figure, one can compare the IL spectra calculated using as reference either the free field (without ground) or the field produced by a finite impedance surface (with ground). Three heights of the microphone for the two surfaces previously described have been analyzed. The dashed lines in fig. 5 show the IL calculated considering $p_{tot} = p_0 + p_s$ in eq. (4), *i.e.*, the obtained acoustic field considering the source and the finite impedance surface. On the other hand, the continuous lines represent the IL calculated considering $p_{tot} = p_0$, *i.e.*, free field (without the surface). In the case of the rigid surface (figs. 5(a1), (b1) and (c1)) one can see the increasing of the attenuation properties of the SC when the rigid surface is considered. In the case of the finite impedance surface there is not a relevant variation in the size of the ΓX pseudogap when the surface is considered.

Concluding remarks. – We have shown both numerically and experimentally the interaction between the attenuation properties of both a SC and a finite impedance surface. We have focused our analysis on the case where the axis of the rigid cylinders that form the SC are perpendicular to the surfaces. For this realistic case we have found a good agreement between both the numerical predictions and the experimental data measured using 3DReAMS. Both the EA, due to the presence of the finite impedance surface, and the band gap of the SC interact in order to show a combined effect that depends on the frequency and on the relative position between the measuring point and the position of the source. We have analyzed this interaction from the point of view of the attenuation properties of the SC, finding that for the case of rigid surfaces the combined effect is relevant and it has to be taken into account. However, for finite impedance surfaces with high absorption values, the interaction practically disappears and the attenuation properties of the SC in the measuring points are only dependent on the periodicity of the array as well as on the number of scatterers. The results shown

in this work can be useful to design attenuation devices based on periodic materials as SC acoustic barriers as well as for the design of experiments in which the effect of the surface could interact with the transmission properties of SC.

* * *

This work was supported by MCI Secretaría de Estado de Investigación (Spanish Government) and FEDER funds, under grant MAT2009-09438. VR-G is grateful for the support of "Programa de Contratos Post-Doctorales con Movilidad UPV (CEI-01-11)".

REFERENCES

[1] Kushwaha M., Halevi P., Dobrzynski L. and Djafari-Rouhani B., *Phys. Rev. Lett.*, **71** (1993) 2022.
[2] Sigalas M. and Economou E., *Solid State Commun.*, **86** (1993) 141.
[3] Cervera F., Sanchis L., Sánchez-Pérez J., Martínez-Sala R., Rubio C. and Meseguer F., *Phys. Rev Lett.*, **88** (2002) 023902.
[4] Yang S., Page J. H., Liu Z., Cowan M. L., Chan C. and Sheng P., *Phys. Rev. Lett.*, **93** (2004) 024301.
[5] Feng L., Liu X., Chen Y., Huang Z., Mao Y., Chen Y., Zi J. and Zhu Y., *Phys. Rev. B*, **72** (2005) 033108.
[6] Cummer S. A. and Schuring D., *N. J. Phys.*, **9** (2007) 45.
[7] Sánchez-Pérez J. V., Caballero D., Martínez-Sala R., Rubio C., Sánchez-Dehesa J., Meseguer F., Llinares J. and Gálvez F., *Phys. Rev. Lett.*, **80** (1998) 5325.
[8] Sánchez-Pérez J., Rubio C., Martínez-Sala R., Sánchez-Grandia R. and Gómez V., *Appl. Phys. Lett.*, **81** (2002) 5240.
[9] Pérez-Arjona I., Sánchez-Morcillo V. J., Redondo J., Espinosa V. and Staliunas K., *Phys. Rev. B*, **75** (2007) 014304.
[10] Swintec N., Robillard J. F., Bringuier S., Bucay J., Muralidharan K., Vasseur J. O., Runge K. and Deymier P. A., *Appl. Phys. Lett.*, **98** (2011) 103508.
[11] Kushwaha M., Halevi P., Martínez G., Dobrzynski L. and Djafari-Rouhani B., *Phys. Rev. B*, **49** (1994) 2313.
[12] Romero-García V., Sánchez-Pérez J. V. and Garcia-Raffi L. M., *J. Appl. Phys.*, **108** (2010) 044907.
[13] Laude V., Achaoui Y., Benchabane S. and Khelif A., *Phys. Rev. B*, **80** (2009) 092301.
[14] Rayleigh L., *Philos. Mag.*, **34** (1892) 481502.
[15] Poulton C. G., Movchan A. B., McPhedran R. C., Nicorovici N. A. and Antipov Y. A., *Proc. R. Soc. London, Ser. A*, **456** (2000) 2543.
[16] Zalipev V. V., Movchan A. B., Poulton C. G. and McPhedran R. C., *Proc. R. Soc. London, Ser. A*, **458** (2002) 1887.
[17] Platts S. B., Movchan N. V., McPhedran R. C. and Movchan A. B., *Proc. R. Soc. London, Ser. A*, **458** (2002) 2327.
[18] Guenneau S., Poulton C. and Movchan A. B., *Proc. R. Soc. London, Ser. A*, **459** (2003) 643.
[19] McPhedran R. C. and Movchan A. B., *J. Mech. Phys. Solids*, **42** (1994) 711.
[20] Movchan A. B., Nicorovici N. A. and McPhedran R. C., *Proc. R. Soc. London, Ser. A*, **453** (1997) 643.
[21] Martin P. A., *Multiple Scattering. Interaction of Time-Harmonic Waves with N Obstacles* (Cambridge University Press, UK) 2006.
[22] Linton C. and McIver P., *Handbook of Mathematical Techniques for Wave/Structure Interactions* (CRC Press) 2001.
[23] Chen Y. Y. and Ye Z., *Phys. Rev. E*, **64** (2001) 036616.
[24] Taflove A., in *Advances in Computational Electrodynamics: The Finite-Difference Time-Domain Method*, edited by Soukoulis C. M. (Artech House, London) 1998.
[25] Ihlenburg F., *Finite Element Analysis of Acoustic Scattering* (Springer-Verlag, New York) 1998.
[26] Romero-García V., Sánchez-Pérez J. V. and Garcia-Raffi L. M., *J. Phys. D: Appl. Phys.*, **44** (2011) 265501.
[27] Krynkin A., Umnova O., Chong A. Y., Taherzadeh S., Attenborough K. and Sánchez-Pérez J. V., arXiv:1102.3159v2 (2011).
[28] Berenguer J., *J. Comput. Phys.*, **114** (1994) 185.
[29] Taherzadeh S. and Attenborough K., *J. Acoust. Soc. Am.*, **105** (1999) 2039.